ELSEVIER

Journal of Pharmaceutical and Biomedical Analysis
17 (1998) 651–663

JOURNAL OF
PHARMACEUTICAL
AND BIOMEDICAL
ANALYSIS

Quantitative imaging microscopy for the sensitive detection of administered metal containing drugs in single cells and tissue slices—a demonstration using platinum based chemotherapeutic agents

R.J. Mauthe, E. Sideras-Haddad, K.W. Turteltaub, G. Bench *

Biological and Biotechnology Research Program and Center for Accelerator Mass Spectrometry, Lawrence Livermore National Laboratory, Livermore, CA 94550, USA

Received 2 July 1997; received in revised form 6 October 1997; accepted 6 October 1997

Abstract

We describe the use of Nuclear microscopy (microbeam PIXE) for the quantitative micron scale analysis of platinum based chemotherapeutic agents in individual cells and tissue slices. We demonstrate that microbeam PIXE has the sensitivity and accuracy to quantitatively measure the uptake of the chemotherapeutic agent *cis*-diamminedichloroplatinum(II) (cisplatin) and monitor other endogenous metal contents in single cells in a time- and dose-dependent fashion. Additionally, the technique can quantitatively image therapeutic levels of cisplatin and cisplatin analogs including *cis*-diammine[1,1-cyclobutanedicarboxylato]platinum(II) (carboplatin) in tissues from an animal model. This quantitative imaging microscopy has general application for the sensitive measurement of metal containing drugs/compounds at the cellular level and allows the study of cellular distribution and mechanism of action related to toxic response and cell function.

Keywords: Cisplatin; Carboplatin; Nuclear Microscopy; Particle induced X-ray emission (PIXE); Single cell analysis; Quantitative metal detection

1. Introduction

Biological systems integrate metals into many of the processes crucial to cell viability and the spatial relationships of metals with associated organelle functions is important for understanding cellular processes. Examples include the use of zinc in DNA recognition proteins that are important to gene expression and DNA repair [1–3], and the use of iron in the active site of enzymes that oxidize environmental and endogenous chemicals in cells. Although metals are required at trace levels, most metals are toxic or carcinogenic at higher levels (i.e. selenium).

Metal-containing drugs are also widely used in the treatment of specific cancers [4]. *cis*-diamminedichloroplatinum(II) (cisplatin) and cis-

*Corresponding author. Tel.: +1 510 4235155; fax: +1 510 4237884; email: bench1@llnl.gov

0731-7085/98/$19.00
PII S0731-7085(97)00225-2

platin analogs including *cis*-diammine[1,1-cyclobutanedicarboxylato] platinum(II) (carboplatin), for example (see Fig. 1), are the therapy of choice for testicular and ovarian cancers [5,6]. These platinum drugs are thought to act through the formation of DNA adducts in the cancerous cells. Cisplatin forms mainly intrastrand crosslinks which are thought to be molecular targets recognized by transcription factors and thereby disrupting normal RNA or DNA synthesis [7–9]. The clinically inactive *trans* isomer of cisplatin, *trans*-diamminedichloroplatinum(II) (transplatin), also forms DNA adducts, but these DNA adducts are not recognized by the same transcription factors and do not disrupt cellular-functions [9–11].

Although these platinum containing drugs are effective for a number of cancer types, the nephrotoxicity and neurotoxicity of these drugs has been a constant concern. Despite, cisplatin analogs, such as carboplatin, and improved dosing regimens to reduce kidney associated side effects the toxicity of these drugs is still not completely understood. One factor hindering improved understanding of the nephrotoxic effects of these platinum containing chemotherapeutic drugs (and, in general, the roles that metals play in cellular processes) is that presently used analysis techniques often cannot provide accurate quantitation of metals with sufficient spatial resolution in biological matrices. For instance, although fluorescent dye or monoclonal antibody staining techniques often provide excellent spatial information they are not quantitative and often only indicate the presence of a metabolite. In contrast, bulk material analyses, such as atomic absorption spectroscopy or inductively coupled plasma mass spectrometry, can quantify samples of sufficient size but do not yield spatial information required for analyses of tissue histology.

For improved understanding of the roles that metals and metal containing drugs play in cell viability it is desirable to use techniques that can quantitatively measure trace metal distributions with sub-cellular spatial resolution within the context of the histological organization of tissues. Quantitation of very specific metal detection at the micron scale or better should allow a quantitative comparison of results and processes on the function of the metals at the cellular level. Here we describe the use of such a technique called nuclear microscopy and demonstrate its utility for the sensitive detection of administered metal containing drugs by examining the uptake of platinum based chemotherapeutic agents in Chinese hamster ovary (CHO) cells and rat kidney tissue. We first demonstrate the sensitivity, dynamic range and quantitation of the technique by measuring platinum contents in rat blood plasma spiked with cisplatin. We subsequently, show how the technique can measure the uptake of cisplatin and monitor other metal contents within single cells in a time- and dose-dependent fashion. Finally, we show how nuclear microscopy can quantitatively image the localization of platinum and other metals within kidney tubule cross-sections from rats administered therapeutic levels of cisplatin and carboplatin.

2. Methods

2.1. Nuclear Microscopy

Nuclear microscopy [12] using particle induced X-ray emission (or microbeam PIXE) [13] is an X-ray fluorescence technique that uses MeV energy proton beams focused to micron sized dimensions to interrogate microscopic specimens. It provides accurate quantitation, simultaneous multi-element detection and is capable of sub-micron scale spatial resolution whilst maintaining down to part per million (by weight) or mg g^{-1} elemental sensitivity. The use of one method to quantitate and localize numerous metals is particularly advantageous when comparing two or more processes related to metal concentrations. Moreover, the penetration depth of MeV protons ($\sim$100 mm in biological material for 3 MeV protons) allows microbeam PIXE to measure the total elemental contents within a cell or tissue section.

Lawrence Livermore National Laboratory operates a nuclear microprobe which can currently focus 100 pA, MeV energy proton beams down to $<$1 mm beam spot diameters [14].

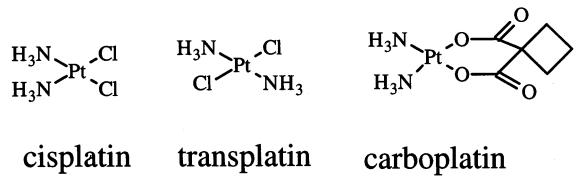

Fig. 1. Structure of cisplatin, transplatin and carboplatin.

With this system, ~ 50 keV H^- ions are produced by an off-axis duoplasmatron ion source and accelerated and stripped in a tandem electrostatic accelerator to produce MeV energy H^+ ions (protons). These ions subsequently pass through the field of an energy analyzing magnet and an aperture which helps control the energy stability of the accelerator. The nuclear microscope lies 0.5 m downstream of the energy stabilization aperture. At the entrance to the microscope, the central portion of the beam core is first selected and then further collimated by sets of slits before being focused onto the specimen by magnetic quadrupole lenses. The focused beam is scanned over the sample by electrostatic deflection in a point by point raster mode. The beam dwells at a particular sample location until a preset amount of integrated current dose has been recorded before stepping onto the next beam location. Fig. 2 shows a schematic diagram of the nuclear microprobe analysis of biological samples at Livermore.

Incident protons interact primarily with atomic electrons in the specimen creating vacancies in inner shell orbitals. When a vacancy is filled by an outer shell electron, the excess energy resulting from the transition can be released as an X-ray photon whose energy is characteristic of the emitting atom. This technique is called proton induced X-ray emission or PIXE. In nearly all PIXE experiments, solid state energy dispersive detectors are used to detect the emitted X-rays produced during specimen irradiation. As the beam is scanned across the sample, X-ray energy spectra are stored for each beam location. After data acquisition, maps of element concentrations can be generated from this data and X-ray spectra from beam locations corresponding to any region of interest can be extracted for quantitative analysis [15].

Microbeam PIXE causes minimal alteration to the sample [16]. The MeV ion energies cause negligible sputtering of material from the specimen surface and very low radiation damage. The use of $\leq$ nA beam currents and a scanned beam minimizes thermal damage to the specimen. For our analysis of biological specimens, target currents and scanning parameters are chosen so that detected X-ray yields from elements of interest remain constant as a function of integrated dose. Specimen deformation and changes in the spatial distribution of elements are then usually not dis-

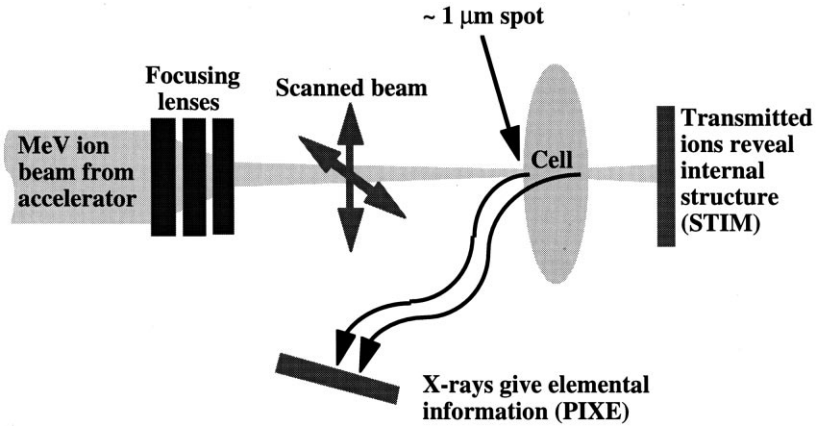

Fig. 2. Schematic diagram of microbeam particle induced X-ray emission (PIXE) and scanning transmission ion microscopy (STIM) analysis of biological tissue at Livermore. The MeV energy beam from an accelerator is focused onto the specimen by magnetic quadrupole lenses. The focused beam is scanned over the sample by electrostatic deflection in a point by point raster mode.

cernible on the micron scale. This choice of irradiation parameters helps to ensure the quantitative accuracy of PIXE measurements.

In quantitative X-ray analysis it is necessary to extract characteristic X-ray peak areas (or yields) from the elements of interest in the X-ray spectrum and to convert these yields into elemental concentrations. To obtain accurate and precise quantitative PIXE analysis of X-ray spectra, computational PIXE spectrum fitting codes are used [17]. This is possible because of the simple physics involved for PIXE and the accurate databases available. With this approach a wide range of specimen types may be handled with a small suite of thin film standards used to calibrate the detector efficiency. The Livermore nuclear microprobe system and spectrum analysis code [18] have been tested on a range of certified standards and have a quantitative accuracy of better than 5% for biological samples [18].

Other nuclear microprobe analysis techniques, such as scanning transmission ion microscopy (STIM) [19], can also be performed to complement microbeam PIXE data. With STIM the residual energy of ions after passing through the specimen is measured by particle detectors located directly behind the sample. Because of the simple physics involved in ion energy loss mechanisms and the accurate data bases available ion energy losses can be readily converted into specimen projected densities enabling determination of the specimen mass. Consequently, STIM data is often collected to normalize PIXE data so that target thicknesses can be accurately measured in order to obtain quantitative PIXE elemental concentrations [19,20]. Because STIM is nearly 100% efficient, beam currents can be reduced to a few thousand ions per second by using small aperture sizes in the microprobe system. Fine spatial resolution can thus be achieved. This efficiency and resolution makes it possible to observe fine features in thin samples [20]. The fine spatial resolution, ~ 0.3 μm, can provide a rapid, histological assessment of the specimen (i.e. area, shape and projected thickness).

Nuclear microscopy is one of a variety of particle and X-ray microprobe techniques that has been used for elemental localization studies in biological tissues [21]. Three of the most directly competitive techniques include electron probe X-ray analysis, X-ray induced X-ray fluorescence and secondary ion mass spectrometry [22]. Each of these techniques has certain advantages and limitations when compared with other methods. However, in general, only microbeam PIXE has the ability to make several quantitative measurements simultaneously at μg g^{-1} range sensitivity and micron scale spatial resolution while minimally affecting the specimen.

Electron probe X-ray analysis utilizing energy dispersive X-ray detectors can be performed at 10 nm spatial resolutions for very thin specimens but has detection sensitivities of around one thousand μg g^{-1} [22]. Further, electron beams do not sample the whole specimen volume but are limited to surface or near surface analysis for all but the thinnest of samples. X-ray induced X-ray fluorescence can have 0.1 μg g^{-1} element detection sensitivities, but it is typically limited to spatial resolutions greater than 10 μm [22]. Secondary ion mass spectrometry (SIMS) has ~ 1 μm spatial resolution in its imaging mode, is an ideal tool for performing isotope ratio measurements and possesses element sensitivities down to 0.01 μg g^{-1}, but is prone to problems of quantitative accuracy in elemental content determination [20]. SIMS does not sample the whole specimen volume and its destructive nature frequently exacerbates the difficulties associated in obtaining quantitative accuracy.

2.2. Nuclear microprobe analysis

All samples were examined using the nuclear microprobe facility located at the Lawrence Livermore National Laboratory [14]. PIXE and STIM data were obtained using incident 3 MeV proton microbeams. X-rays were detected with an energy dispersive Si(Li) detector that subtended a solid angle of ~ 120 msr to the specimen. The detector was located at an angle of 135° with respect to the incident beam. Charge was collected in a biased Faraday cup locatedbehind the sample. X-rays were recorded in list mode along with coincident beam spatial co-ordinates arising from scanning the beam electrostatically over the sample in a

point by point raster mode. To minimize specimen heating effects during irradiation the beam was repeatedly rastered over the interrogated region. Within each raster pass up to 0.1 nC of charge was deposited to each beam location.

For STIM, residual ion energies were measured with a retractable charged particle silicon surface barrier detector located approximately 5 cm directly behind the sample and in front of the Faraday cup. The surface barrier detector was retracted from the path of the beam during PIXE measurements (the million fold higher beam currents used for PIXE rapidly result in catastrophic detector damage [23]). Residual ion energies were recorded in list mode along with coincident beam spatial co-ordinates arising from scanning the beam electrostatically over the sample in a point by point raster mode. The residual energy of 19 ions was measured at each beam location. The median value of these 19 residual ion energies was selected to represent the average residual energy of the ion beam after traversing the sample [23]. Energy thicknesses were converted to specimen projected densities assuming the composition of the biological material to be $C_5H_9O_2N$ [23]. Such an approximation has been shown to be accurate to within a few percent for a wide variety of biological matrices [23].

2.3. Sensitivity and dynamic range of PIXE for cisplatin dosing of blood plasma

To determine the sensitivity of PIXE for the detection of platinum in biological matrices, 3 ml of blood was collected by cardiac puncture from a F-344 male rat (approximately 150 g and 10 weeks of age purchased from Simonsen Laboratories (Gilroy, CA)) euthanized with CO_2. EDTA (2.5 μmol) was added to the blood to prevent coagulation. The blood was centrifuged at $3000 \times g$ for 5 min to pellet blood cells from the plasma and 350 μl aliquots of the resulting plasma fraction were pipetted into four separate test tubes. Cisplatin (SIGMA, St. Louis MO) was dissolved in 0.9% sodium acetate to a concentration of 1.0 mg ml^{-1} and serial dilutions in 0.9% sodium acetate were subsequently performed to obtain additional solutions containing 0.1 and 0.01 mg ml^{-1} cisplatin immediately prior to use. Plasma standards of cisplatin were prepared at concentrations of 28, 2.8 and 0.28 μg ml^{-1} by adding 10 μl of the 1.0, 0.1 and 0.01 mg ml^{-1} stock solutions respectively to three of the 350 μl plasma samples. As a control 10 μl of 0.9% sodium acetate was mixed into the fourth aliquot of plasma. Each of the four plasma samples was subsequently centrifuged at $3000 \times g$ for 2 min to ensure homogeneity. The concentration of platinum (μg g^{-1}) in each of these final plasma samples was determined assuming that the EDTA, 0.9% sodium acetate and the plasma had unit density (i.e. 1.0 g cm^{-3}).

Aliquots (10 μl) of each plasma sample were pipetted onto separate ultra clean 1 μm thick, transparent nylon foils stretched over a 15 mm diameter hole in a plastic support frame. All target frames used for these studies had been stored in a lyophilizer for 48 h prior todeposition of the plasma to help ensure removal of volatile elements and compounds. Following deposition of blood plasma each target frame was rapidly plunged into and stored in liquid nitrogen. All four target frames were subsequently freeze dried in a lyophilizer. Once lyophilized all four samples were stored in a clean, ultra-dry environment prior to microbeam analysis.

The mass of each target frame was measured using a microbalance both before deposition of blood plasma solution and after lyophilization. For each target frame the mass of lyophilizedmaterial was determined from the difference between the two microbalance mass measurements. The mass of lyophilized material on each frame was typically around 1 mg and had an uncertainty of less than 5% percent. The analyzed cisplatin concentration in the lyophilized material on each frame was determined by multiplying the cisplatin concentration in the corresponding blood plasma solution by the ratio of the mass of 10 μl of blood plasma to the mass of the lyophilized material. For these calculations, the blood plasma samples were again assumed to have unit density. This methodology produced targets of lyophilized blood plasma containing cisplatin concentrations of 290 ± 20, 30 ± 2 and 2.8 ± 0.2 μg g^{-1} dry weight. These prepared dry weight concentrations

of cisplatin in blood plasma were most probably accurate to within 10%.

For microbeam PIXE analysis of each of the plasma samples beam currents of up to 2 nA focused down to spot sizes of 10×10 μm were scanned over a 1×1 mm^2 area of the lyophilized plasma. Areas were irradiated with an exposure of up to 5 μC. Data were reduced off-line [15] and X-ray spectra were analysed with the PIXEF spectrum fitting code [18]. To cross check the detector's X-ray detection efficiency a thin film platinum standard of thickness 41.7 ± 2.1 μg cm^{-2} was also analysed. The microbeam PIXE analysis yielded a measured platinum thickness of 42.4 ± 1.8 μg cm^{-2} for this standard. Following PIXE analysis STIM was used to measure the energy thickness of the irradiated region on each target. STIM measurements revealed that incident 3 MeV protons typically lost ~ 200 keV in traversing the lyophilized plasma. The energy thickness measurements were used to correct the platinum L X-ray yield measurements for X-ray attenuation within the plasma samples and for variation of X-ray production cross-section with ion energy in order to obtain platinum concentrations in μg g^{-1} dry weight. The platinum concentrations were then multiplied by the molecular weight of cisplatin and divided by the molecular weight of platinum in order to obtain the measured weight concentration of cisplatin in each lyophilized plasma sample.

2.4. Time and dose dependent analysis of cisplatin in CHO cells

To show how microbeam PIXE can measure the uptake of cisplatin and monitor other metal contents within single cells in a time- and dose-dependent fashion we have exposed Chinese hamster ovary cells to cisplatin for up to 24 h. The cells in suspension were exposed to 1, 2 and 5 μg ml^{-1} cisplatin which approximate in-vivo therapeutic concentrations.

UV5P3 Chinese hamster ovary (CHO) cells [24] were grown as suspension cultures in 15 ml glass roller tubes using MEM-α media with 10% fetal calf serum at 37°C with continuous rolling action. Cells were passaged 24 h prior to treatment with cisplatin so that the cells were rapidly dividing. Immediately prior to cisplatin treatment, the cells were refed with 10 ml fresh media. Three cell cultures at a cell density of $\sim 20{,}000$ cells ml^{-1} were treated with 1 ml of 10 μg ml^{-1}, 20 μg ml^{-1} or 50 μg ml^{-1} cisplatin solutions for up to 24 h. In each case the dosing solution was made in 0.9% NaCl. Media samples (1 ml) were removed immediately prior to treatment resulting in final cisplatin concentrations of 1, 2 and 5 μg ml^{-1} to the three cultures. Media samples (1 ml) were also removed at 2, 6 and 24 h time points. Each 1 ml media sample was centrifuged ($4124 \times g$ for 5 min) to pellet the CHO cells. The resulting pellet was then washed twice to remove the incubating medium by re-suspending the CHO cells in 0.15 M sodium acetate, pH 7.4 (2 ml) and centrifuging the cells at $4124 \times g$ for 5 min. Washing the cells could result in the possibility of loss of cellular cisplatin due to re-equilibrium of the cisplatin with the sodium acetate medium. Consequently, following each wash 5 μl aliquots of the used washing medium was mounted on nylon foils, frozen and lyophilized as described above. PIXE analyses of these freeze dried samples did not reveal the presence of platinum down to minimum detectable limits of 5 μg g^{-1}. Approximately 5 μl of the final CHO cell pellet was pipetted onto ultra-clean, 1 μm thick, transparent nylon foils as described above and stored frozen in liquid nitrogen in an aluminium block. The aluminium block was subsequently lyophilized under a vacuum of 10^{-2} Torr for 6 h. Once lyophilized all samples were stored in a clean, ultra-dry environment prior to microbeam analysis. Optical studies revealed that the characteristic morphology of the CHO cells was retained after lyophilization (data not shown).

For microbeam PIXE analysis of individual CHO cells 3 MeV proton beam currents of ~ 0.6 nA were focused down to spot sizes of $\sim 2.5 \times 2.5$ μm and were scanned over $\sim 40 \times 40$ μm^2 areas. Each scan area contained one CHO cell of diameter ~ 15 μm. Areas were irradiated with an exposure of up to 5 μC. On each target frame (representing a particular dose-incubation time co-ordinate pair) five cells were analysed. Data were reduced off-line [15] and X-ray spectra corre-

sponding to the CHO cell within each scan region were extracted and analysed with the PIXEF spectrum fitting code [18]. In a similar vein to the analysis of the blood plasma samples the detector's X-ray detection efficiency was cross-checked using iron, copper, zinc and platinum thin film standards. Following PIXE analysis STIM was used to measure the energy thickness of the irradiated regions on each target. STIM measurements revealed that incident 3 MeV protons lost up to ~ 40 keV in traversing the freeze dried CHO cells. The energy thickness measurements were used to correct the elemental X-ray yield measurements for X-ray attenuation within the tissue sections and for variation of X-ray production cross-section with ion energy in order to obtain $\mu g\ g^{-1}$ dry weight concentrations.

2.5. Uptake of platinum containing compounds by rat kidney tubules

Although platinum containing drugs are effective for a number of cancer types, the nephrotoxicity of these drugs has been a concern. Despite, cisplatin analogs, such as carboplatin, and improved dosing regimens to reduce side effects the toxicity of these drugs is still not properly understood. To determine if the varying nephrotoxicity of the different cisplatin analogs may be related to different rates of uptake or transport of these drugs by constituent kidney tubule cells we have quantitatively imaged the micron scale localization of platinum and other metals within kidney tubule cross-sections from rats administered therapeutic levels of cisplatin and carboplatin.

F-344 male rats (approximately 150–175 g and 10–12 weeks of age) were purchased from Simonsen Laboratories (Gilroy, CA). The animals were housed in an AAALAC accredited facility maintained on a 12 h light/dark cycle. The animals were housed in polycarbonate cages on hardwood bedding with free access to food and water. Three rats were dosed by intraperitoneal (IP) injection with 6.5 mg kg^{-1} cisplatin, two animals were dosed with 6.5 mg kg^{-1} transplatin, two animals were dosed with 6.5 mg kg^{-1} carboplatin, two animals were dosed with 65 mg kg^{-1} carboplatin and two additional rats were administered saline as a vehicle control. In each case, the dosing solution was made immediately prior to dosing in 0.9% NaCl at a concentration of 1 mg ml^{-1} or 10 mg ml^{-1} (for 65 mg kg^{-1} dose). The 6.5 mg kg^{-1} cisplatin dose and 65 mg kg^{-1} carboplatin dose (owing to its reduced toxic effects larger doses of carboplatin are often administered) correspond to the therapeutic doses typically used for the treatment of human cancers.

The rats were euthanized by CO_2 asphyxiation 2 h after treatment and immediately dissected. Whole kidneys were removed and sliced into several cubes of dimensions $\sim 2 \times 2 \times 2$ mm. Immediately after dissection, these cubes were rapidly plunged into liquid nitrogen and subsequently stored in a -80°C freezer until they were cryosectioned. Frozen cubes of tissue were cryo-sectioned at -27°C using stainless steel blades in a Leica CM 1800 cryo-microtome to obtain 8 μm thick frozen hydrated sections. A fresh blade was used for each frozen kidney cube. The sections were subsequently mounted onto pre-cooled transparent nylon membranes stretched over a 15 mm diameter hole in a plastic support frame while still within the cryochamber. To ensure rigid attachment of the tissue sections to the nylon membrane the sections were placed with slight pressure over two ~ 200 μm thick parallel lines of carbon paint pre-cooled to -270°C. These carbon paint lines were separated by ~ 2 mm and were deposited onto the nylon membrane ~ 30 s before attachment of the tissue sections. The mounted frozen hydrated sections were then stored in a liquid nitrogen cooled aluminium block within the cryo-chamber. The aluminium block was subsequently lyophilized under a vacuum of $< 10^{-3}$ Torr for 6 h. Once lyophilized all samples were stored in a clean, ultra-dry environment prior to microbeam analysis.

For microbeam PIXE analysis of kidney tubules 3 MeV proton beam currents of 0.1–0.8 nA were focused down to spot sizes of $\sim 1 \times 1$–3×3 μm and were scanned over $\sim 70 \times 70$ μm^2 areas of the prepared kidney tissue sections. Areas were irradiated with an exposure of up to 6 μC. For the transplatin, 6.5 mg kg^{-1} carboplatin, 65 mg kg^{-1} carboplatin and saline doses two kidney tubule cross-sections were analysed from each

kidney. For the cisplatin dose, two animals each had two tubule cross-sections from each kidney analysed, while only one tubule cross-section from one kidney was analysed for the remaining animal subjects. Data were reduced off-line [15] and X-ray spectra corresponding to the tubule cross-section within each scan were extracted and analysed with the PIXEF spectrum fitting code [18]. In a similar vein to the analysis of the blood plasma samples the detector's X-ray detection efficiency was cross-checked using thin film standards of iron, copper, zinc, platinum, calcium fluoride and potassium chloride. Following PIXE analysis STIM was used to measure the energy thickness of the irradiated regions on each target. STIM measurements revealed that incident 3 MeV protons typically lost ~ 20–30 keV in traversing the freeze dried kidney tissue sections. The energy thickness measurements were used to correct the elemental X-ray yield measurements for X-ray attenuation within the tissue sections and for variation of X-ray production cross-section with ion energy in order to obtain μg g^{-1} dry weight concentrations.

2.6. Data Presentation

Comparisons of the different platinum compounds and other metal contents within cells or kidney tubules were assessed by Students t-tests where appropriate. A significance level of < 0.01 was considered meaningful. A significance level of > 0.05 was not considered meaningful while a significance level between 0.01 and 0.05 was considered to be inconclusive.

3. Results and Discussion

3.1. Sensitivity and dynamic range of PIXE for cisplatin dosing of blood plasma

The prepared and measured dry weight cisplatin concentrations in the four lyophilized plasma samples are shown in Table 1. Fitting the data using the least squares method with a function in the form $y = mx + c$ where y is the cisplatin concentration measured by PIXE and x is the prepared cisplatin concentration yields a gradient (m) of 0.892 and an intercept (c) of -0.727. The coefficient of correlation is 0.99998. The $\sim$ 10% difference between the measured and prepared values most probably arises from a systematic error in the preparation of the plasma samples and/or derivation of the prepared cisplatin concentrations within these samples (such as the assumption of solution unit density). The data indicate that PIXE has excellent linearity for the detection of platinum in biological matrices over the range of ~ 1 to several hundred μg g^{-1} dry weight. The data also indicates that background levels in the control plasma sample are below the minimum detection limits of PIXE. The minimum detection limit for platinum was estimated from the sample that had a prepared cisplatin concentration of 2.8 μg g^{-1}. The minimum detection limit(mdl) of platinum was taken to be $3.29x$ the square root of the background signal below the platinum Lα peak. For a dose of 5 μC to the plasma sample, the mdl of platinum was determined to be 0.3 μg g^{-1} dry weight which yields a mdl for cisplatin of ~ 0.5 μg g^{-1}dry weight.

Table 1
The prepared and measured cisplatin concentrations in the four lyophilized plasma samples in units of mg g^{-1} dry weight.

Prepared concentration	Measured concentration
290 ± 20	258 ± 13
30 ± 2	25 ± 1
2.8 ± 0.2	2.7 ± 0.3
0	Not detected

3.2. Time and dose dependent analysis of cisplatin in CHO cells

Table 2 shows the measured platinum concentrations in CHO cells incubated in 1, 2 and 5 μg ml^{-1} cisplatin for 2, 6 and 24 h as well as control data sets. Each data point is expressed as the mean $\pm$ SD of measurements from five cells. In the control data sets for which CHO cells were not incubated in cisplatin, platinum was not detected in any cells. The platinum minimum detec-

Table 2
Measured platinum and copper concentrations (expressed as a mean ± SD of measurements from five cells) in Chinese hamster ovary cells incubated in 1, 2 and 5 mg ml^{-1} (first column) cisplatin for 2, 6 and 24 h (first row).

	0 h	2 h	6 h	24 h
Platinum (μg ml^{-1})				
1[1]	Not detected	22 ± 13	54 ± 11	150 ± 41
2	Not detected	37 ± 8	122 ± 20	188 ± 36
5	Not detected	72 ± 12	186 ± 38	208 ± 43
Copper (μg ml^{-1})				
1	104 ± 17	107 ± 19	76 ± 25	86 ± 18
2	86 ± 15	74 ± 18	81 ± 14	62 ± 21
5	94 ± 21	80 ± 26	43 ± 19	52 ± 13

All concentrations are in mg g^{-1} dryweight.

tion limit for these measurements was < 5 μg g^{-1}.

Both a time-dependent and dose-dependent increase in the uptake of cisplatin into individual CHO cells is observed. Some cytotoxicity (judged by low cell counts) was observed for the 5 μg ml^{-1} dose at the 6 and 24 h time points likely due to the high levels of macromolecular damage. Subcellular elemental mapping of the CHO cells revealed a homogeneous distribution of platinum within the cell compartment. This observation agrees with the fact that cisplatin binds to numerous intracellular nucleophilic sites, in the cytosol as well as in the nucleus. This is consistent with the observation that only 1% of the total cellular platinum generally binds to DNA [25].

As PIXE possesses simultaneous multi-element detection we also analysed the content of iron, copper and zinc within the CHO cells. The levels of iron and zinc remained constant at approximately 200 ± 50 and 350 ± 70 μg g^{-1} respectively for the various doses and exposure times and were not statistically significant ($P > 0.05$). In a similar vein the levels of copper in the ovary cells for both the 1 and 2 μg ml^{-1} doses as a function of exposure time to cisplatin are notsignificantly different ($P > 0.05$). However, for the 5 μg ml^{-1} dose the level of copper appears to follow a decreasing trend as a function of exposure time to cisplatin. Copper levels decreased from 94 ± 21 μg g^{-1} in the control to 52 ± 13 μg g^{-1} at 24 h in the 5 μg ml^{-1} dose ($P < 0.01$). Although the cytotoxicity observed for the 5 μg ml^{-1} dose at the 6 and 24 h time points may account for the decreasing copper levels, these results are consistent with the reduction of copper in the kidneys of cisplatin treated rats [26–28] which has been attributed to an inhibition of reabsorption of copper in the kidney tubules or an inhibition in the synthesis of renal metallothionein. Interestingly, when a human ovary adenocarcinoma cell line which is resistant to cisplatin was studied using nuclear microprobe methods [29] slightly increased copper levels associated with decreased platinum levels were observed in relation to a cisplatin sensitive cell line. However, regardless of the mechanism resulting in the decreased copper concentration observed in the present study, the data show how microbeam PIXE can provide quantitative time and dose response data at the single cell level on several elements simultaneously.

3.3. Uptake of platinum-containing compounds in rat kidney tissue sections

Fig. 3A shows a low resolution optical micrograph recorded before microbeam irradiation of a portion of sectioned kidney tissue containing a kidney tubule cross-section. This sample was from a rat dosed with 6.5 mg kg^{-1} cisplatin. Fig. 3B shows corresponding images of phosphorus, sulfur, chlorine, potassium, iron, copper, platinum and total X-ray distributions resulting from this irradiation. Fig. 3C shows a high resolution optical micrograph of the same region of the sample

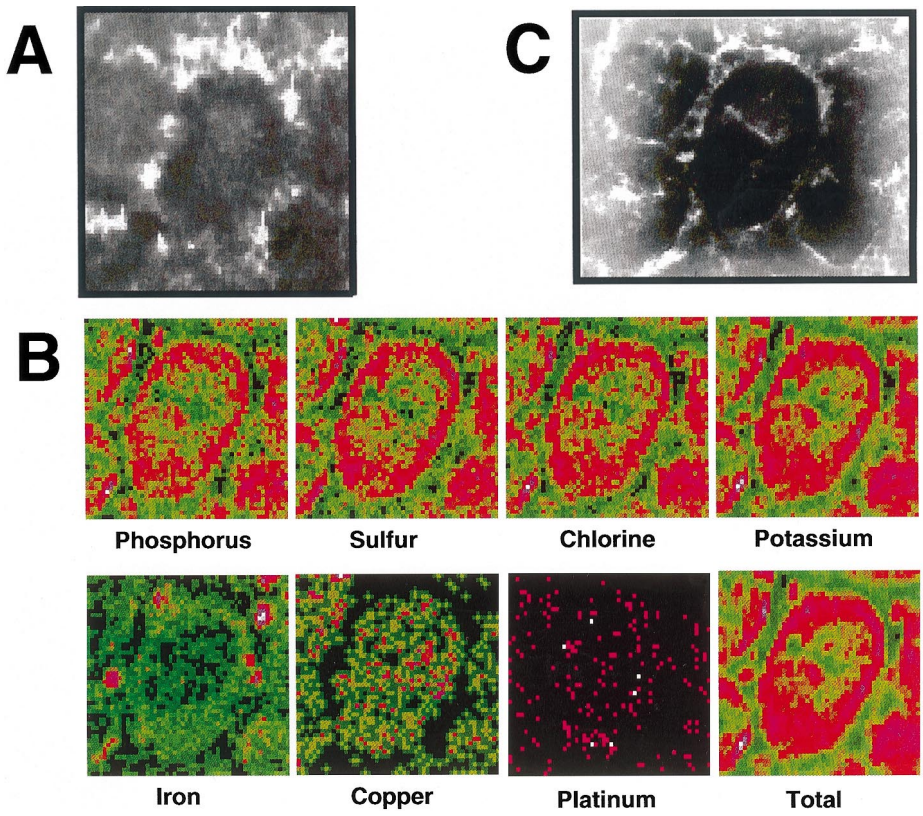

Fig. 3. Images of a freeze dried tissue section of rat kidney containing a cross-section through a kidney tubule. (A) Low resolution optical micrograph recorded before microbeam radiation. The image size is $\sim 100 \times 100$ μm^2. (B) P, S, Cl, K, Fe, Cu, Pt and total X-ray distributions from the same sample area resulting from a 4 μC irradiation to the tissue section. The data was obtained with a 3 MeV proton beam focused down to a beam spot of 1.5 μm diameter. In each image the color scale is related to element concentration. The color scale ranges from black (minimum concentration) through light green, dark green, red, purple to white (maximum concentration). The range that the color scale spans in each image differs. The image sizes are 65×69 μm^2 and consist of 48×52 pixels. (C) High resolution optical micrograph of the same sample area recorded after all microbeam analysis. The image size is $\sim 105 \times 85$ μm^2. The darkened region in the center of the image that contains the kidney tubule cross-section corresponds to areas irradiated with the microbeam during sample positioning and analysis.

after microbeam analysis. Table 3 shows the measured platinum concentrations (expressed as a mean $\pm$ SD) within rat kidney sections from dosing with 6.5 mg kg^{-1} cisplatin, 6.5 mg kg^{-1} transplatin, 6.5 mg kg^{-1} carboplatin, 65 mg kg^{-1} carboplatin and saline (control). In the control samples platinum was not detected in any kidney tubule. The platinum minimum detection limit for these measurements was < 5 μg g^{-1}.

The ratio of the platinum concentration within kidney tubules of rats administered the 65 mg kg^{-1} carboplatin dose to rats administered the 6.5 mg kg^{-1} carboplatin dose is 7.7 ± 2.0 indicating a dose-dependent increase in drug content within constituent kidney tubule cells.

For the 6.5 mg kg^{-1} doses the platinum concentration within kidney tubules arising from the cisplatin and transplatin doses are significantly different to that from the carboplatin dose ($P < 0.01$). However, when the doses are normalized for the molecular weights of carboplatin (371.3 g mol^{-1}) and cisplatin or transplatin (300.0 g mol^{-1}) the number of moles of platinum in a 6.5 mg kg^{-1} carboplatin dose is 80.8% of the number of moles of platinum in a 6.5 mg kg^{-1} cisplatin or transplatin bolus. Thus, normalizing the platinum

Table 3
Measured (μg g^{-1}) dry weight platinum concentrations (expressed as a mean ± SD) within rat kidney tubules from dosing with cisplatin, transplatin, carboplatin, carboplatin and saline (control).

IP dose	Number of animals	Number of tubules	Pt concentration
Cisplatin (6.5 mg kg^{-1})	3	9	174 ± 30
Transplatin (6.5 mg kg^{-1})	2	8	186 ± 27
Carboplatin (6.5 mg kg^{-1})	2	8	125 ± 23
Carboplatin (65 mg kg^{-1})	2	8	956 ± 178
Saline (control)	2	8	Not detected

data for the amount of platinum drug delivered yields Conc(carboplatin)/Conc(transplatin) = 0.8 ± 0.2, Conc(carboplatin)/Conc(cisplatin) = 0.9 ± 0.2 and Conc(transplatin)/Conc(cisplatin) = 1.1 ± 0.2 within the kidney tubule cross-sections (where Conc(x) is the normalized concentration of drug x). Further, Students t-tests reveal that there are no significant differences between the normalized cisplatin, carboplatin and transplatin contents in the kidney tubule cross-sections at significance levels of at least 0.05. Differences in the elemental concentrations of P, S, Cl, K Fe, Cu and Zn within kidney tubules were also not statistically significant ($P > 0.05$) for the exposure regimes to saline, cisplatin, carboplatin and transplatin at this early time point following cisplatin exposure. Previous studies observing a decrease in bulk copper levels associated with cisplatin treatment in rat kidneys observed a time-dependent decrease in copper levels increasing to at least 30 days with only very small decreases at 24–72 h [27].

The equal distribution of the three platinum-containing drugs in constituent kidney tubule cells is consistent with previous studies [30] and supports the hypothesis that cisplatin's toxicity and therapeutic value may result from differences in glomerular filtration, the reactivity of the compounds within the kidney tubules (including oxidative damage) or the molecular mechanism involving a difference in handling of the DNA adducts [9,30,31].

Although no significant differences in the concentration of the other metals examined were observed in these tissue sections, this data only shows metal contents after 2 h of exposure. We have not as yet examined the long term affects of these platinum containing drugs on endogenous metal content. However, we have performed broad beam ($\sim 1 \times 1$ mm^2) PIXE analyses on kidney tissues obtained from a rat given a 6.5 mg kg^{-1} IP dose and euthanized 15 h later to determine if PIXE had sufficient sensitivity to detect platinum at later time points. The results revealed that PIXE had sufficient sensitivity to measure platinum levels at the 15 h time point and yielded a cisplatin concentration of ~ 40 μg g^{-1}. Further studies may be able to test the hypothesis that cisplatin causes disturbances in metal (Ca, Na, K, Zn) concentrations hypothesized to be related to cisplatin's acute renal toxicity [9,27,32–34]. Pursuit of such studies with PIXE may reveal a better understanding on the nephrotoxicity (and neurotoxicity) of cisplatin and may be able to improve the efficacy of chemotherapeutic treatments by determination of the concentration of platinum and other metals within the kidney tubules following modified dosing regimens or drug analogs.

This data demonstrates the utility of microbeam PIXE for the sensitive detection of administered metal containing drugs by examining the uptake of platinum based chemotherapeutic agents in tissues from animal models. The ability of PIXE to simultaneously quantitate the concentration of several metals in tissue samples allows for preservation of histological information and allows us to identify that the platinum is specifically within the tubule structures. To the best of our knowledge, this is the first demonstration of the microbeam PIXE technique to quantitatively image platinum in tissues from an animal model given therapeutic levels of platinum containing cancer treatments. Furthermore, the sensitivity of the microbeam PIXE technique is sufficient to

potentially measure therapeutic levels of cisplatin and cisplatin analogs in human subject tissue biopsies. The technique is not limited to the sensitive measurement of metal containing drugs/compounds at the cellular level but allows studies such as changes in endogenous metals within cells in response to bacterial pathogens or any chemical or environmental challenge.

4. Conclusion

In these studies we have demonstrated the utility of using microbeam PIXE for the quantitative analysis of platinum containing chemotherapeutic agents in individual cells and tissue slices. Microbeam PIXE has the sensitivity and accuracy to quantitatively measure the uptake of cisplatin and monitor other trace metal content within single cells in a time- and dose-dependent fashion as well as image the localization of platinum within kidney tubule cross-sections from rats administered therapeutic levels of cisplatin and carboplatin. In addition to the determination of platinum compound content microbeam PIXE allows for the simultaneous determination of other element concentrations within the specimen. This quantitative imaging microscopy has general application for the sensitive detection of metal containing drugs/compounds at the cellular level and allows a very good comparison of results and processes on the function of endogenous metals in single cells and tissue slices.

Acknowledgements

The authors would like to thank Mark Roberts and Dan Morse for assistance with nuclear microprobe operation and data collection. The authors are also very much indebted to Becky Wu for supplying the CHO cells used in these studies and to Debbie Cumrine at the Veterans Affairs Medical center in San Francisco for use of the cryo-microtome facility and for many useful discussions concerning the preparation of freeze dried tissue sections for elemental microanalysis. This work was performed under the auspices of the U.S. Department of Energy by Lawrence Livermore National Laboratory under contract W-7405-ENG-48 and partially supported by NIH grant ESO9705.

References

[1] A.S. Prasad, Nutrition 11 (1995) 93–99.
[2] H.C. Nelson, Curr. Opin. Genet. Dev. 5 (1995) 180–189.
[3] T. Tamura, Y. Konishi, Y. Makino, K. Mikoshiba, Neurochem. Int. 29 (1996) 573–581.
[4] W. Pratt, R. Ruddon, W. Ensminger, J. Maybaum, The Anticancer Drugs, Oxford University Press, New York, 1994.
[5] R. Young, C. Perez, W. Hoskins, in: Cancer: Principles and Practice of Oncology, V. DeVita, S. Hellman, S. Rosenberg, (Eds.), Lippincott, Philadelphia, 1993, pp. 1226–1263
[6] L. Einhorn, J. Richie, W. Shipley, in: Cancer: Principles and Practice of Oncology, V. DeVita, S. Hellman, S. Rosenberg, (Eds.) Lippincott, Philadelphia, 1993, pp. 1126–1151
[7] B.A. Donahue, M. Augot, S.F. Bellon, D.K. Treiber, J.H. Toney, S.J. Lippard, J.M. Essigmann, Biochemistry 29 (1990) 5872–5880.
[8] G. Chu, E. Chang, Science 242 (1988) 564–567.
[9] D.K. Treiber, X. Zhai, H.M. Jantzen, J.M. Essigmann, Proc. Natl. Acad Sci. U. S. A. 91 (1994) 5672–5676.
[10] P.M. Pil, S.J. Lippard, Science 256 (1992) 234–237.
[11] J.H. Toney, B.A. Donahue, P.J. Kellett, S.L. Bruhn, J.M. Essigmann, S.J. Lippard, Proc. Natl. Acad Sci. U. S. A. 86 (1989) 8328–8332.
[12] J.A. Cookson, A.T.G. Ferguson, F.D. Pilling, J. Radioanal. Chem., 12 (1972) 39.
[13] S.A.E. Johansson, J.L. Campbell, PIXE–A Novel Technique for Elemental Analysis, Wiley, Chichester, 1988.
[14] M.L. Roberts, G. Bench, D.W. Heikkinen, D.H. Morse, P.H. Bach, A.E. Pontau, Nucl. Instrum. Methods B104 (1995) 13–18.
[15] A.J. Antolak, G.S. Bench, D.H. Morse, Nucl. Instrum. Methods B85 (1994) 597.
[16] W. Maenhaut, Scanning Microsc. 4 (1990) 43.
[17] J.L.Campbell, W. Maenhaut, E. Bombelka, E. Clayton, K., Malmqvist, J.A. Maxwell, J.Pallon, J. Vandenhaute, J. Nucl. Instrum. Methods, B14 (1986) 204.
[18] A.J. Antolak, G.S. Bench, Nucl. Instrum. Methods B90 (1994) 596.
[19] H.W. Lefevre, R.M.S. Schofield, G. Bench, G.J.F. Legge, Nucl. Instrum. Methods B54 (1991) 363–370.
[20] G. Bench, Ph.D. Thesis, (1991),University of Melbourne, Australia
[21] W. Mueller-Klieser, S. Walenta, Histochem. J. 25 (1993) 407.

[22] R.W. Linton, J.G. Goldsmith, Biol. Cell 74 (1992) 147.
[23] H.W. Lefevre, R.M.S. Schofield, J.C.Overley, J.C. McDonald, Scanning Microsc., 1 (1987) 879–889.
[24] R.W. Wu, E.M. Wu, L.H. Thompson, J.S. Felton, Carcinogenesis 16 (1995) 1207–1213.
[25] P.A. Andrews, S.B. Howell, Cancer Cells 2 (2) (1990) 35.
[26] R.W. Mason, I.R. Edwards, Toxicology 37 (1985) 267–274.
[27] R.W. Mason, I.R. Edwards, Biochem. Pharmacol. 34 (1985) 2575–2577.
[28] R.S. DeWoskin, J.E. Riviere, Toxicol. Appl. Pharmacol. 112 (1992) 182–189.
[29] R. Ortega, P. Moretto, A. Fajac, J. Benard, Y. Llabador, M. Simonoff, Cell. Mol. Biol. 42 (1996) 77–88.
[30] M.J. McKeage, Drug Saf. 13 (1995) 228–244.
[31] M.H. Hanigan, B.C. Gallagher, P.T. Taylor, Jr., Am. J. Obstet. Gynecol. 175 (1996) 270–273.
[32] P.I. Campbell, I.A. al-Nasser, Toxicology 114 (1996) 11–17.
[33] J.G. Zhang, L.F. Zhong, M. Zhang, X.L. Ma, Y.X. Xia, W.E. Lindup, Hum. Exp. Toxicol. 13 (1994) 89–93.
[34] M.G. Cherian, S.B. Howell, N. Imura, C.D. Klaassen, J. Koropatnick, J.S. Lazo, M.P. Waalkes, Toxicol. Appl. Pharmacol. 126 (1994) 1–5.